Guiding of Relativistic Electron Beams in Solid Targets by Resistively Controlled Magnetic Fields

S. Kar,[1] A. P. L. Robinson,[2] D. C Carroll,[3] O Lundh,[4] K. Markey,[1] P. McKenna,[3] P. Norreys,[2] and M. Zepf[1,*]

[1]School of Mathematics and Physics, Queen's University, Belfast, BT7 1NN, United Kingdom
[2]Central Laser Facility, Rutherford Appleton Laboratory, Chilton, OX11 0QX, United Kingdom
[3]Department of Physics, University of Strathclyde, Glasgow, G4 0NG, United Kingdom
[4]Department of Physics, Lund Institute of Technology, P.O. Box 118, S-22100 Lund, Sweden

(Received 24 September 2008; published 5 February 2009)

Guided transport of a relativistic electron beam in solid is achieved experimentally by exploiting the strong magnetic fields created at the interface of two metals of different electrical resistivities. This is of substantial relevance to the Fast Ignitor approach to fusion energy production [M. Tabak *et al.*, Phys. Plasmas **12**, 057305 (2005)], since it allows the electron deposition to be spatially tailored—thus adding substantial design flexibility and preventing inefficiencies due to electron beam spreading. In the experiment, optical transition radiation and thermal emission from the target rear surface provide a clear signature of the electron confinement within a high resistivity tin layer sandwiched transversely between two low resistivity aluminum slabs. The experimental data are found to agree well with numerical simulations.

DOI: 10.1103/PhysRevLett.102.055001 PACS numbers: 52.57.−z, 52.38.Kd

The generation of relativistic (fast) electron beams is a very important aspect of intense ($I\lambda^2 > 10^{18}$ W cm^{-2}) laser-solid interactions. The subsequent propagation of the fast electrons through dense plasma has been extensively studied and is of significant interest due to potential technological applications of laser-generated fast electrons such as the Fast Ignitor [1,2], high energy density physics [3], laser induced radiation sources [4], and particle acceleration [5,6].

The Fast Ignitor relies on efficiently coupling the energy of a short-pulse laser to heat the hot-spot region in the dense deuterium-tritium fuel to temperatures ~10 keV [1,2], which initiates a burn wave that propagates through the rest of the compressed fuel. In the basic concept this is achieved by first converting the laser energy into a relativistic electron beam and transporting the electron beam to the hot spot [7]. The typically large angular divergence of the electron beam [8,9] poses significant design constraints on Fast Ignition, which underline the importance of finding regimes in which electron transport can be controlled. Briefly, for Fast Ignition, the "hot spot" within the fuel must have an areal density $\rho r_{\mathrm{HS}} > 0.6$ g cm^{-2}, temperature $kT \sim 10$ keV, and densities of >300 g cm^{-3} [10]. Divergent beam transport therefore constrains the laser spot size to be smaller than the hot-spot radius $r_{\mathrm{HS}} \sim$ 15–20 μm and limits the distance between electron beam source and fusion fuel to a few tens of μm. Larger standoff distances will decrease the coupling efficiency and consequently require more laser energy to reach ignition. Since the maximum ignition pulse duration is given by stagnation time of the compressed fuel (~10 ps), it is clear that the fuel parameters and coupling efficiency fully determine the minimum intensity of the ignition laser. For 1 μm laser wavelength divergent electron beam transport therefore implies laser intensities $>10^{20}$ W cm^{-2} [10] and a classical stopping distance longer than the optimum (and hence degraded efficiency). The electron energy can then only be controlled by varying the remaining free parameter—the laser wavelength—which is undesirable from a practical perspective [11]. Finally, while the current design of the cone guided implosions [12] has been shown to be an effective approach to achieve efficient coupling in small scale experiments [13], a full scale implosion may require a substantially thicker cone tip in order to prevent the cone from being destroyed prematurely. This implies a larger standoff distance and possible coupling losses using divergent transport. Divergent beam transport therefore leads to undesirable design bottlenecks regarding the electron beam energy, laser design, and target design. However, if controlling the divergence of the electron beam were possible, the laser intensity and standoff distance become free design parameters—substantially enhancing the chances of success for Fast Ignition. This Letter reports the first experimental evidence that shows that the divergence of relativistic electron beams in a solid density plasma can indeed be controlled, thus providing the level of target design flexibility that may be crucial to the success of the Fast Ignitor.

The experiment reported here is based on a recent theoretical study by Robinson and Sherlock [14], who proposed a radically different route to artificially forcing collimated beam transport to occur. This new scheme is based on using a structured target in which the resistivity η (through the atomic number Z) varies in the direction transverse to the electron beam propagation. The physical basis of this is that to leading order the magnetic field grows according to

$$\frac{\partial \mathbf{B}}{\partial t} = \eta \nabla \times \mathbf{j} + (\nabla \eta) \times \mathbf{j}. \quad (1)$$

The second term in the right-hand side of Eq. (1) implies that a magnetic field will grow at resistivity gradients which acts to drive electrons into the regions of higher resistivity. Therefore a target that consists of a central

"core" of material with higher resistivity than the surrounding material should naturally enhance the growth of magnetic field that acts to collimate the fast electrons along the central "core." The key in the technique is to maintain the sign of the resistivity gradient across the boundary, which could be ensured by choosing the "core" metal of higher atomic number than the surrounding metal.

While Robinson and Sherlock [14] proposed cylindrical geometry, our proof-of-principle experiment used a "sandwich" target [a thin slab of tin (Sn) with aluminum (Al) either side] irradiated by the laser as shown in Fig. 1(a). It was designed to give a clear evidence of the effect by showing different divergence in the confined dimension (transverse to the Sn layer) and the nonconfined dimension (along the Sn layer). Clearly, the change in geometry will lead to a different field geometry; however, numerical investigations were initially performed to ensure that this approach was an appropriate configuration for a proof-of-principle experiment.

As Eq. (1) suggests, the target does not need to be cylindrically symmetric, and strong resistivity gradient along the Al/Sn boundary will lead to rapid magnetic field growth and consequently guiding of the fast electrons should still occur in the "sandwich" target geometry, albeit the fast electrons are only strongly confined in one dimension—normal to the Sn slab. The much weaker magnetic confinement parallel to the Sn slab should result in an elongated electron beam profile at the target rear surface. We developed and employed a 3D hybrid code, called ZEPHYROS, which uses similar approximations and methods to the hybrid code of Davies [15] (i.e., a particle-based hybrid code with static background plasma), to generate some predictions that could be compared to the experimental results.

Two targets were simulated. One (the reference target) consisted of pure Al. The other target modeled was the Al-Sn-Al slab geometry as employed in the experiment [see Fig. 1(a)]. Simulation setup is described in the appendix of this Letter. As expected, the simulation for the Al target produced a fairly uniform electron distribution of ~ 100 μm full width at half maximum (FWHM) at the rear surface (i.e., $z = 200$ μm plane) as shown in Fig. 2(a). On the other hand, the asymmetrical electron distribution obtained for the case of sandwich target can be seen in Fig. 2(b). Because of the resistivity gradient across the interfaces, the generated strong magnetic walls at the interfaces confine the electron within it, whereas some of the electrons managed to escape before the strength of the magnetic field could be sufficient to confine them. The magnetic field lines at the two interfaces join together at the top and bottom (along Y axis) of the simulation box passing through the tin layer. This part of the magnetic field has similar strength to that in the interfaces and would inhibit further spreading of the electrons along the tin layer (Y axis). In practice, however, this does not result in a significant reduction in divergence when compared to the pure aluminum case, and the difference in divergence provides a clear signature of the guiding effect in the experiment.

The experiment was performed at Rutherford Appleton Laboratory employing VULCAN petawatt laser system. After reflection from a plasma mirror [16], the laser pulse delivered ~ 150 J of energy on target in FWHM duration of 1 ps. The laser was focused to a 20 μm spot diameter, reaching a peak intensity of 10^{20} W cm^{-2} on target at 10° angle of incidence. The guiding target consisted of a

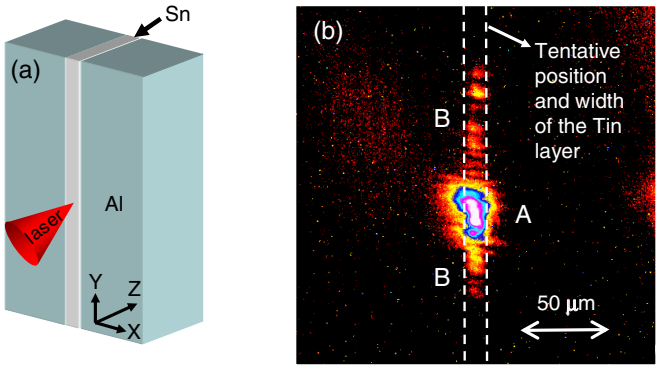

FIG. 1 (color online). (a) Schematic of the Al-Sn-Al sandwich target employed in the experiment. (b) The experimentally obtained time-integrated image of optical transition radiation from the Al-Sn-Al target rear surface at 527 nm. Labels A and B represent, respectively, the central bright spot and the dim line feature (along Y) on both sides of A.

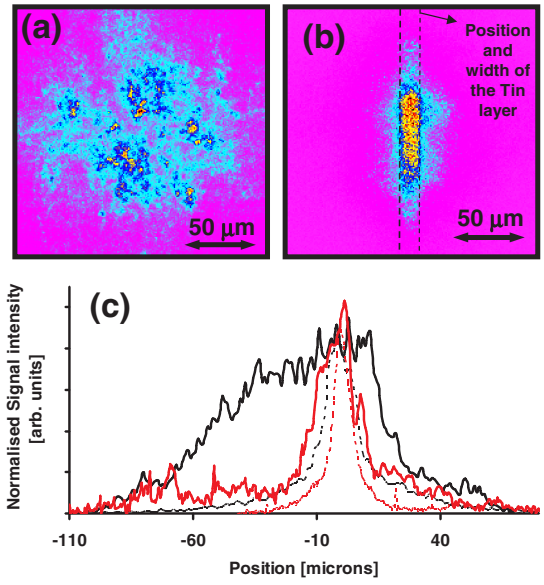

FIG. 2 (color online). (a),(b) The square of the spatial distribution of the hot electron density at the rear surface of pure aluminum and modeled sandwich target obtained from 3D hybrid code, respectively. (c) Comparison between lineouts of (b) (black lines) and Fig. 1(b) [gray (red) lines] along X (thick lines) and Y (thin broken lines) directions.

12 μm thick Sn foil sandwiched between two Al slabs of 5×10 mm cross section and 200 μm thick along the target normal [Fig. 1(a)]. The laser polarization and plane of propagation are in the XZ plane [as designated in Fig. 1(a)] and the ratio between atomic numbers and cold electrical resitivities of Sn and Al are 4:1 and 4.5:1, respectively [17], ensuring that the resistivity gradient is maintained throughout the interaction. The target rear surface was lapped to a roughness of $\sim$50 nm rms and coated with a submicron gold layer to ensure a uniform surface for the optical emission. The reference target was a 200 μm thick Al foil with rear Au coating and similar rear surface roughness. Optical emission from the target rear surface was collected by a $f/6$ lens to allow time-integrated images of the coherent optical transition radiation (OTR) emitted at twice the laser frequency (527 ± 5 nm [18]) and thermal emission (700 ± 20 nm) to be simultaneously recorded on CCD cameras using optical interference filters. The spatial resolution of the images at 527 and 700 nm were 4 and 5.5 μm, respectively.

The OTR image for the guiding target in Fig. 1(b) shows a line of strong emission with an aspect ratio at $1/e^2$ level of approximately 5:1. The transverse FWHM and the orientation of the emission in the experimental data agree well with the Sn layer of the guiding target fielded in the experiment. The large aspect ratio observed with the guiding target is in excellent agreement with the simulated electron beam profile shown in 2(b) and is in stark contrast to both the near circular distribution (aspect ratio 1.1:1) observed in both experiment and simulation for the aluminum reference target 2(a). This is in agreement with previous investigations over a wide parameter range that also show that slab targets typically display near circular OTR patterns [19–21]. The emission at 527 nm is mainly the result of microbunching at half the laser wavelength (1054 nm) produced via $\vec{J} \times \vec{B}$ mechanism [19,22]. The emission from the microbunches is coherent and the intensity scales with the square of the number of bunched electrons. The lineouts of the coherent OTR data and square of the electron beam distribution in Fig. 2(c) show that the simulation and experiment are quantitatively well matched in $1/e^2$ width. However, the intensity distribution along the Sn layer for the guiding target deviates somewhat from the simulations. This may be due to the initial divergence of the beam being less smooth than assumed in the simulations. Another possibility is that the initial bunching of the electron beam at $2\omega_{\text{laser}}$ is more substantially affected by the guiding fields off the main propagation axis. Since the OTR intensity depends on the temporal structure of the electron beam, any loss of bunching, e.g., due to the path length differences resulting from the guiding, would lead to deviations between the simulated electron beam density and OTR emission profile. However, the overall agreement between the simulation and data is still excellent.

Further evidence of the beam collimation was obtained from the images taken at 700 nm. OTR emission at this wavelength is very weak [18] and the time-integrated image is dominated by thermal emission. The thermal emission observed with the guiding target [Fig. 3(a)] shows an elliptical heating pattern with the long axis aligned to the direction of the Sn layer, albeit with a much reduced aspect ratio when compared to the OTR emission at 527 nm. By contrast, the reference target displays a uniform circular heating profile [see Fig. 3(b)] at its rear surface. The long axis (Y axis) of the heating pattern obtained with the guiding target has the same FWHM as

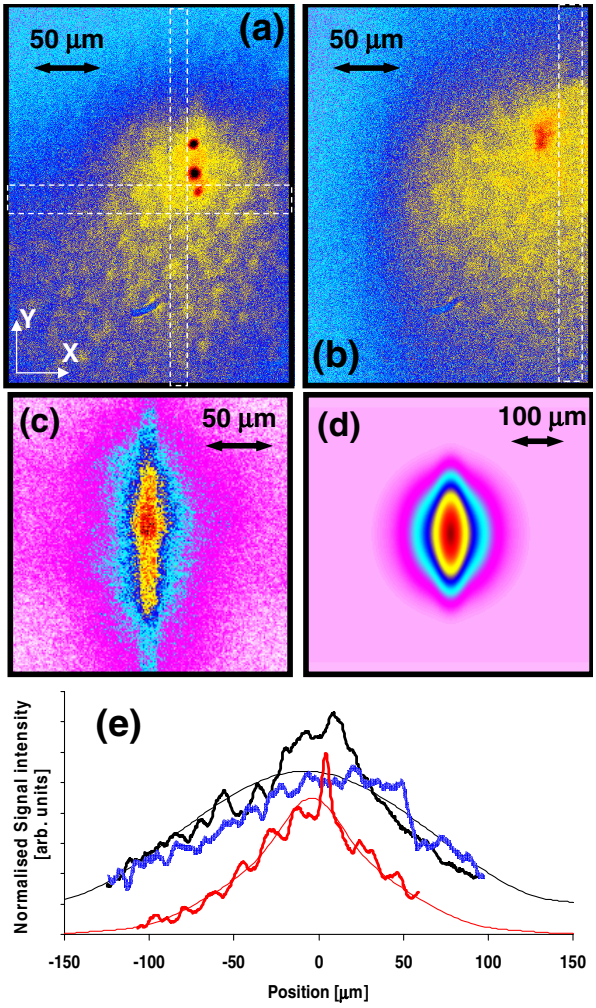

FIG. 3 (color online). Thermal emission images observed at 700 nm for guiding target (a) and reference target (b). (c) 2D temperature profile of the rear side of the guiding target obtained at $t = 1.5$ ps from the 3D hybrid code. (d) Time-integrated heating pattern in the wavelength range 700 ± 20 nm, obtained by postprocessing the ZEPHYROS output shown in (c). (e) Comparison of simulated (thin lines) and observed heating patterns (thick lines) along the x axis [gray (red) line] and y axis [thick black solid line for (a) and thick blue dotted line for (b)]. Dashed lines in (a) and (b) indicate area integrated for the lineouts.

the circular heating profile observed with the reference target [Fig. 3(e)], whereas it is roughly double the short axis (x axis) FWHM.

In order to compare the experimentally obtained heating profiles with the simulation, the temperature profiles obtained at $t = 1.5$ ps with ZEPHYROS [Fig. 3(c)] were post-processed using the 2D hydrodynamic code POLLUX [23]. The evolution of the heated region was simulated for 3 ns with a temperature profile output at every 100 ps. For every time step, the emitted thermal radiation (in the range 700 ± 20 nm wavelength) from the surface was computed by approximating the thermal emission using Plank's law of blackbody radiation. The simulated time-integrated thermal emission profile thus obtained is shown in Fig. 3(d). It has FWHM of 80 and 150 μm along X and Y axes, respectively, in good agreement with the experimental results [Fig. 3(e)].

In conclusion, guiding of relativistic electron beams has been demonstrated by employing a scheme where strong magnetic field is generated along resistivity gradients incorporated in the target design. The relativistic electron beam is shown to follow the contours of the boundary closely, suggesting that cylindrical collimation (as suggested by Robinson and Sherlock [14]) and also focusing of the electron beam are possible using suitably shaped resistivity boundaries. This scheme may have substantial positive impact on the Fast Ignitor approach to fusion energy production, by enhancing coupling efficiencies of the relativistic electron beam to the fusion fuel and by relaxing some geometrical constraints on the target design.

Authors would like to acknowledge grant support from EPSRC and the Royal Society and support from the QUB workshop and RAL staff.

Appendix: Simulation setup.—The simulations were carried out in a $200 \times 200 \times 200$ μm box with the cell size being $1 \times 1 \times 1$ μm. Fast electrons were injected from the $z = 0$ plane with the injection region being centered on $x = y = 100$ μm. This models the laser pulse traveling in the $+z$ direction and incident on the $z = 0$ surface. The transverse absorption profile is determined by $I = \beta I_0 \cos^2(\pi r/2r_{\text{spot}})$, where β is a laser-fast electron conversion efficiency, I_0 is the laser intensity, r is the radial distance from $x = y = 100$ μm, and r_{spot} is the FWHM of laser focal spot. In the simulations, β was set to 0.3, I_0 was set to 10^{20} W cm^{-2}, and r_{spot} was set to 20 μm (these parameters are the same as the experiment). This heating profile was constant over the laser pulse duration which was set to 500 fs. No further injection occurred after this time. The fast electron temperature was determined from the expression given by Wilks *et al.* [24]. The energy of each fast electron was chosen from an exponential probability distribution $f(E) = \exp[-E/\langle E\rangle]/\langle E\rangle$, where $\langle E\rangle$ is the average fast electron energy. The electrons were injected uniformly over a solid angle subtended by $2\theta_{\text{div}}$, which was set to 60°. Roughly 26 000 quasiparticles were injected per time step, which is five quasiparticles per injection cell per time step. In terms of modeling the resistivity and specific heat capacities of the materials, Al was modeled in the same way that Davies modeled Al in Ref. [15] (i.e., a fit to the measurements of Milchberg *et al.* [25]). The resistivity of tin was specified by $\eta(T) = T/[2 \times 10^6 + 3 \times 10^5 T + 100T^{5/2}]$ Ωm, where T is in electron volts. This gives the Spitzer resistivity for fully ionized tin at very high temperatures, and at the low temperatures (around 1 eV, the temperature to which the simulations were initialized) it gives a resistivity which is about 2 times greater than Al at the same temperature [15,25]. The specific heat capacities are determined by the same fit to the Thomas-Fermi model that Davies uses. The simulations were run up to 1.5 ps. Reflective spatial boundaries were used throughout. The reference simulation was carried out with simulation box made of Al. In the case of the Al-Sn-Al target, the sandwiched tin slab was 12 μm thick centered at $x = 100$ μm (the region defined as $94 < x < 106$ μm, $0 < y < 200$ μm, and $0 < z < 200$ μm). The materials were blended slightly (~ 2 μm) at the interfaces (as was done in [14]) due to numerical reasons.

*m.zepf@qub.ac.uk

[1] M. Tabak *et al.*, Phys. Plasmas **12**, 057305 (2005).
[2] S. Nakai and K. Mima, Rep. Prog. Phys. **67**, 321 (2004).
[3] E. M. Campbell, Nucl. Instrum. Methods Phys. Res., Sect. A **415**, 27 (1998).
[4] H. S. Park *et al.*, Phys. Plasmas **13**, 056309 (2006).
[5] M. Borghesi *et al.*, Fusion Sci. Technol. **49**, 412 (2006).
[6] A. Mackinnon *et al.*, Phys. Rev. Lett. **88**, 215006 (2002).
[7] C. Deutsch *et al.*, Phys. Rev. Lett. **77**, 2483 (1996).
[8] J. Green *et al.*, Phys. Rev. Lett. **100**, 015003 (2008).
[9] K. Lancaster *et al.*, Phys. Rev. Lett. **98**, 125002 (2007).
[10] S. Atzeni *et al.*, Phys. Plasmas **15**, 056311 (2008).
[11] HiPER technical design report, www.hiper-laser.org.
[12] P. A. Norreys *et al.*, Phys. Plasmas **7**, 3721 (2000).
[13] R. Kodama *et al.*, Nature (London) **432**, 1005 (2004).
[14] A. P. L. Robinson and M. Sherlock, Phys. Plasmas **14**, 083105 (2007).
[15] J. Davies, Phys. Rev. E **65**, 026407 (2002).
[16] B. Dromey *et al.*, Rev. Sci. Instrum. **75**, 645 (2004).
[17] G. W. C. Kaye and T. H. Laby, *Tables of Physical and Chemical Constants* (Longman, Essex, England, 1995), 16th ed., p. 150.
[18] S. D. Baton *et al.*, Phys. Rev. Lett. **91**, 105001 (2003).
[19] J. J. Santos *et al.*, Phys. Rev. Lett. **89**, 025001 (2002).
[20] H. Popescu *et al.*, Phys. Plasmas **12**, 063106 (2005).
[21] R. Jung *et al.*, Phys. Rev. Lett. **94**, 195001 (2005).
[22] S. C. Wilks *et al.*, Phys. Rev. Lett. **69**, 1383 (1992).
[23] G. J. Pert, J. Comput. Phys. **43**, 111 (1981).
[24] S. C. Wilks *et al.*, IEEE J. Quantum Electron. **33**, 1954 (1997).
[25] H. Milchberg *et al.*, Phys. Rev. Lett. **61**, 2364 (1988).